Comparative study of the breakdown transients of thin Al_2O_3 and HfO_2 films in MIM structures and their connection with the thermal properties of materials

S. Pazos, F. Aguirre, E. Miranda, S. Lombardo, and F. Palumbo

Citation: Journal of Applied Physics **121**, 094102 (2017); doi: 10.1063/1.4977851
View online: http://dx.doi.org/10.1063/1.4977851
View Table of Contents: http://aip.scitation.org/toc/jap/121/9
Published by the American Institute of Physics

Comparative study of the breakdown transients of thin Al_2O_3 and HfO_2 films in MIM structures and their connection with the thermal properties of materials

S. Pazos,[1,2,3] F. Aguirre,[1,2,3] E. Miranda,[4] S. Lombardo,[5] and F. Palumbo[1,2,3,a)]
[1]*Consejo Nacional de Investigaciones Científicas y Técnicas, Godoy Cruz 2290 (C1425FQB), Buenos Aires, Argentina*
[2]*GAIANN, Comisión Nacional de Energía Atómica, Gral. Paz 1499 (1650), San Martín, Provincia de Buenos Aires, Argentina*
[3]*Departamento de Ingeniería Electrónica, Facultad Regional Buenos Aires, Universidad Tecnológica Nacional, Medrano 951 (C1179AAQ), Buenos Aires, Argentina*
[4]*Departament d'Enginyeria Electrònica, Universitat Autònoma de Barcelona, Bellaterra 08193, Spain*
[5]*Istituto per la Microelettronica e Microsistemi (IMM), Consiglio Nazionale delle Ricerche (CNR), Zona Industriale, Ottava Strada, 5, 95121 Catania, Italy*

(Received 24 November 2016; accepted 18 February 2017; published online 3 March 2017)

In this work, the breakdown transients of Al_2O_3- and HfO_2-based metal-insulator-metal (MIM) stacks with the same oxide thickness and identical metal electrodes were compared. Their connection with the thermal properties of the materials was investigated using alternative experimental setups. The differences and similarities between these transients in the fast and progressive breakdown regimes were assessed. According to the obtained results, Al_2O_3 exhibits longer breakdown transients than HfO_2 and requires a higher voltage to initiate a very fast current runaway across the dielectric film. This distinctive behavior is ascribed to the higher thermal conductivity of Al_2O_3. Overall results link the breakdown process to the thermal properties of the oxides under test rather than to dissipation effects occurring at the metal electrodes. *Published by AIP Publishing.*
[http://dx.doi.org/10.1063/1.4977851]

I. INTRODUCTION

In advanced complementary metal-oxide-semiconductor (CMOS) devices, the breakdown (BD) phenomenon of gate dielectrics occurs in the regime of relatively low voltage and high electric field.[1] It is well known that the gate oxide degradation is related to the appearance of a large density of electronic defects promoted by the transport of energetic carriers through the dielectric film.[1,2] That degradation proceeds until a critical density of defects is reached. The consequence of such event is the formation of a localized percolation path spanning the oxide layer. Beyond this point, the oxide BD evolution in very thin films is characterized by a gradual or progressive growth of the leakage current that flows through the device. Both the BD occurrence as well as the particular features of its evolution strongly depend on the applied voltage.[3–5] Besides the relevance of these effects for the scaling of gate dielectrics of transistors in modern CMOS integrated circuits, further insight into the BD physics may also provide a reference framework for different applications of ultra-thin dielectrics, such as, for example, the electrically induced resistive switching (RS) effect. This mechanism, which consists of a kind of reversible BD, has been proposed as the basis for future semiconductor non-volatile memories.[6,7]

Recently, the main physical mechanism behind the progressive BD (PBD) dynamics was identified.[8–10] Briefly, it has been proposed that PBD is closely connected with the energy transfer from the BD path itself to its surrounding atomic network. According to this idea, the high temperature associated with the localized current flow would promote electro-migration of the fastest atomic species among those available, thus contributing to the enlargement of the BD filament. Within this framework, the thermal conductivity of the oxide layer would play a fundamental role in the PBD growth. Other authors[11] suggested in addition that the PBD dynamics in SiO_2 films is connected with the gradual transfer of dissipated power from the bottleneck of the BD path to the electrodes. This not only explains the saturation of the current in the long-run for a constant voltage stress, but also the sustainability of such a large current density in an atomic-size filamentary path. This behavior would be strictly valid for conductance levels close to the quantum conductance limit $G_0 = 2e^2/h$, where e and h are the electron charge and the Planck's constant, respectively. In such case, the BD path behaves as a monomode ballistic conductor with negligible power dissipation.

The influence of the oxide thermal conductivity in the PBD dynamics has been studied for metal-oxide-semiconductor (MOS) stacks with poly-Si[3,4] and metal gate electrodes,[12] with SiO_2, $SiOxNy$, or high-k dielectrics[3–5,8] as gate oxides, and with Si[3,4] and $InGaAs$[8,9,13] substrates. In this work, such a study is extended to the case of metal-insulator-metal (MIM) stacks. Since the metals are high thermal conductivity materials, metal electrodes have a good capability to dissipate the energy arising from the BD path. However, in order to clarify the role played by the metal contacts in MIM stacks during *PBD*, it is important to investigate the energy transfer mechanism from the BD path to its surrounding atomic network.

a)Electronic mail: felix.palumbo@conicet.gov.ar

In this paper, the BD transient in MIM stacks with *Pt* and *Ti/Au* electrodes using 7 nm of ALD-grown high-k dielectrics with different thermal conductivities (Al_2O_3 and HfO_2) were compared. Our results show evidence that the PBD growth is driven by the energy transfer from the BD path to the oxide bulk rather than to the metal electrodes.

II. EXPERIMENTAL

The devices under study are MIM structures with high-k dielectrics and with *Pt* and *Ti/Au* metal contacts. The metal stack was prepared by the lift-off technique. Two sets of devices were fabricated with different high-k dielectrics but with the same metal contacts. Insulating layers of Al_2O_3 (7 nm) and HfO_2 (7 nm) were grown by atomic layer deposition.

Constant Voltage Stress (CVS) experiments were conducted at different voltages, while the current through the stack was measured as the function of time with a current compliance of 100 mA. To monitor the BD transient, two different experimental setups were used. The first one uses a current pre-amplifier and a digital oscilloscope to bias the device and to record the amplified current trace, respectively. This allows sensing the BD current with a time resolution of the order of a few microseconds. Further details about this setup can be found in Refs. 4 and 14. The second configuration is based on a Keithley 2636B source/measurement unit (SMU) and a triaxial-chuck probe station. This configuration provides negligible series resistance, but a limited time resolution of a few milliseconds with a noise background around 100 fA.

Current-voltage (I-V) and voltage-current (V-I) measurements were carried out at dark and at room temperature conditions using the Keithley 2636B SMU.

III. RESULTS

A. Breakdown transients

Figure 1 shows the typical I-t measurements for both sets of samples. Current was monitored using the high-bandwidth setup described in Sec. II until the fast BD event occurred. Figures show the current increase that takes place during the *BD* transient. Figures 1(a)–1(c) correspond to Al_2O_3 MIM stacks measured under different stress voltages, while Figs. 1(d)–1(f) summarize the I-t behavior for the HfO_2 MIM stacks under similar stress conditions. All measurements were performed with a time step of 10 μs and a transimpedance gain of 10^6 V/A, except for Fig. 1(c) that

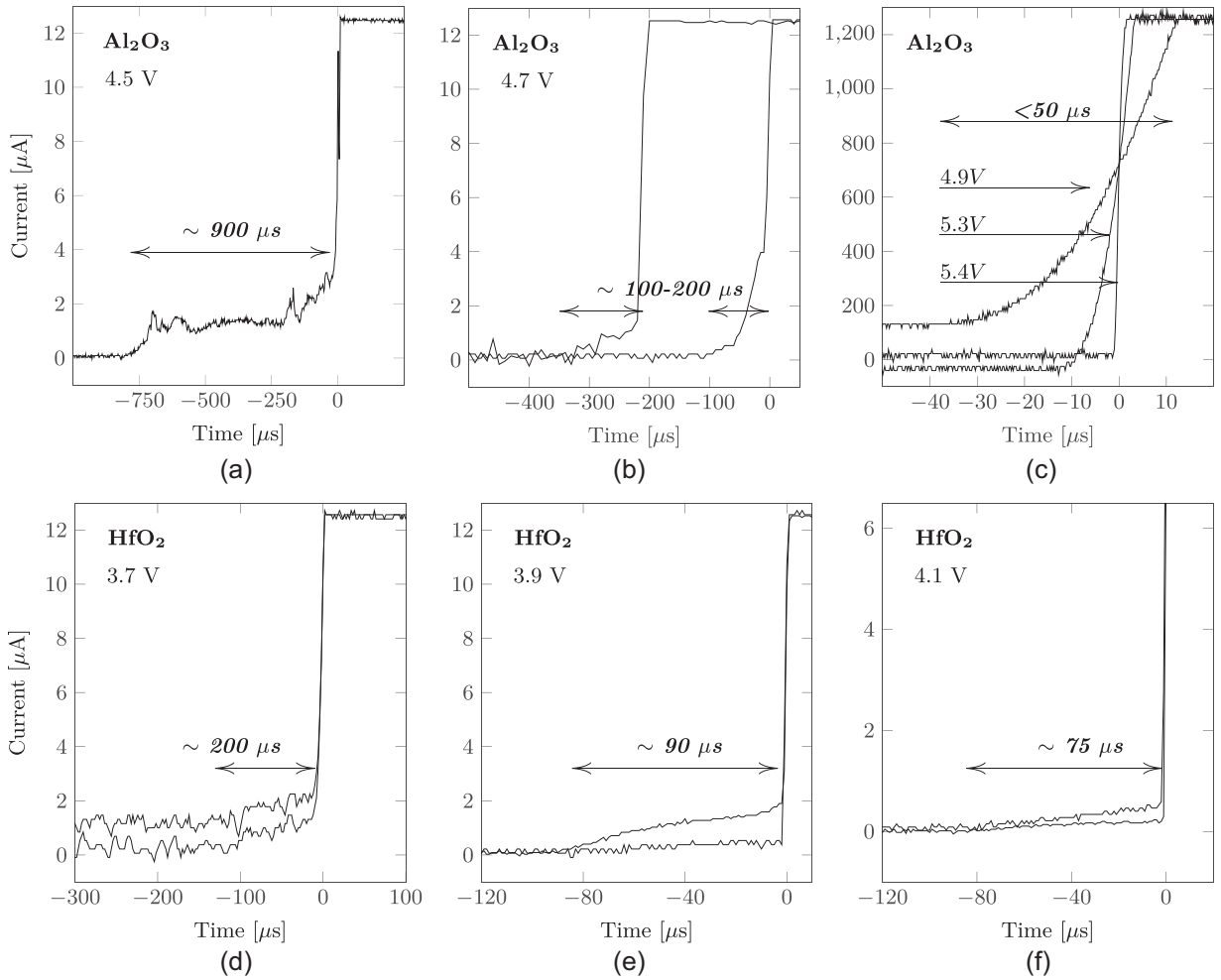

FIG. 1. I-T plots measured with a high bandwidth amplifier for both insulating materials and at different applied voltages. (a)–(c) are for Al_2O_3 samples ranging from 4.5 V to 5.2 V. (d)–(f) are for HfO_2 ranging from 3.7 V to 4.1 V. Arrows indicate the rise time for each set of curves. Curves in (c) were measured at a gain of 10^4 V/A. For the rest, configured gain was 10^6 V/A.

was measured with 1 μs resolution and a gain of 10^4 V/A. All curves show a similar behavior during the BD transient. However, at least two distinctive phases can be recognized in these curves. The first part of the transient is a noisy and progressive growth process well in agreement with that reported in Ref. 14 for SiO_2-based MOS transistors. In the second part of the transient, the gate current jumps abruptly to very high levels in times of the order of microseconds, i.e., limited by the bandwidth of the amplifier. It should be pointed out that only this visualized interval is time resolvable for the employed measurement setup. Before this interval, current levels are below the background noise level (around 0.1 μA). Afterwards, the current runaway is so fast that its capture is limited by the maximum rise time of the amplifier.

Fig. 1(c) shows 3 overlapping plots for Al_2O_3 samples stressed at 4.9 V, 5.3 V, and 5.4 V. I-t curves with steeper slopes, are associated with larger voltages. It is worth noting that the curve corresponding to 4.9 V shows a larger initial current. As demonstrated in Ref. 13, this initial current has no effect on the dynamics of the breakdown event. To quantify the obtained results, the rise-time (t_r) was extracted for each BD transient. t_r is defined as the time required by the current to increase from a level just above the setup noise floor until reaching a steep increase up to the limit of the output dynamic range of the amplifier. This is marked with double arrows in each plot of Fig. 1.

Experimental data show that t_r depends strongly on the applied voltage. Shorter times are obtained at higher applied voltages for both sets of samples. In the case of Al_2O_3, t_r ranges from approximately 900 μs for an applied voltage of 4.5 V in Fig. 1(a) down to less than 50 μs for applied voltages of 5.4 V in Fig. 1(c). For HfO_2 samples, the same behavior is shown but for lower voltages: Fig. 1(d) shows that t_r is around 200 μs for 3.7 V, while in Fig. 1(f), it is close to 70 μs for 4.1 V. From these plots, it should be noticed that the Al_2O_3 samples require higher applied voltages (ca. 1 V higher) than the HfO_2 samples for a similar t_r. Figure 2 shows the rise time t_r as a function of the stress voltage for both sets of devices. The main feature of this plot is that the rise times for Al_2O_3 devices are of the same order as for HfO_2 devices, but at higher applied voltages. Although no statistics assessment is possible with such few measurements, a general trend can be observed consistent with a power or exponential law.

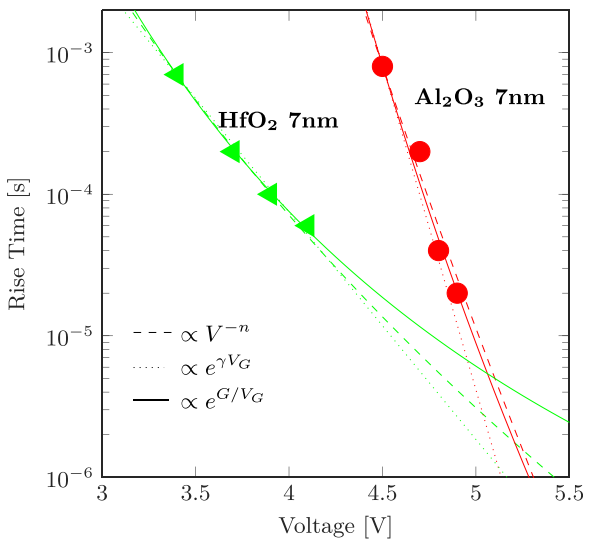

FIG. 2. Extracted t_r for different applied voltages and acceleration model fits for both sets of samples.

The dashed curves in Fig. 2 represent the fitting results of a power law, showing that t_r of Al_2O_3 devices presents a steeper slope ($\propto V^{-41}$) than HfO_2 devices ($\propto V^{-21}$), but with an offset into higher voltages. An extrapolation of these models to lower voltages yields much longer rise-times for Al_2O_3 than for HfO_2. On the other hand, extrapolating the fitting results to higher voltages yields a crossing point around 5.3 V. An in-depth analysis concerning this observation will be carried out at the end of this subsection.

Considering the literature on the breakdown characteristics of high-k insulators in MOS devices as a reference framework, it is found that defects generated during gate oxide stress have long been argued to involve the liberation of charged species by carriers (holes or electrons) followed by the reaction of the liberated species with some precursor such as oxygen vacancies.[15,16] It is the release of charged species through the coupling between vibrational and electronic degrees of freedom that can explain the power-law dependence of defect generation efficiency.[15]

It should be noticed that being the time-to-BD, a current driven phenomenon, the observed deviations in the acceleration factor may be due to different carrier transport in the oxide conduction band (Al_2O_3 and HfO_2 show different band offsets between the dielectric and the metal contact), as was shown for SiO_2 ultra-thin oxides in MOS stacks when considering Direct Tunneling (DT) and Fowler-Nordheim (FN) regimes.[17–19] Regarding the Power-Law exponent value, it is worth noting that, despite a large uncertainty as a result of low sample count, the obtained values are, surprisingly, similar to those reported in the literature for MOS structures.[15,20,21]

Although the study of the acceleration factor is not a topic of this paper, the experimental data of Fig. 2 can also be analyzed in terms of other models.[17] Considering an exponential law of V_G ($t_r \propto e^{\gamma V_G}$), called the E-model, or an exponential law of reciprocal voltage ($t_r \propto e^{G/V_G}$), called the 1/E-model, it is observed that $\gamma(Al_2O_3) = 1.8V^{-1}$ and $\gamma(HfO_2) = 1.1V^{-1}$ for the exponential law of V_G; and $G(Al_2O_3) = 1.6V$ and $G(HfO_2) = 1.1V$ for the exponential law of reciprocal voltage, indicating that the difference in the acceleration factor is also observed.

Although these experiments provide an insight into the progressive nature of the BD transient and show some differences between the two material stacks under study, high bandwidth measurements of Fig. 1 only resolve the final stages of the BD transient, close to the fast current runaway. For very low currents, the output signal of the amplifier falls under the setup noise floor (around 0.1 μA).

In order to study the BD transient in more detail, the whole process including the wear-out phase, must be explored. Therefore, additional CVS measurements were performed for both sets of devices but this time using a commercial SMU with a time resolution of a few milliseconds.

Figures 3(a) and 3(b) show representative measurements at different applied voltages for Al_2O_3 and HfO_2 samples, where the evolution of the current flowing through the MIM structure is shown as a function of time.

I-t curves show the general features of PBD previously reported for MOS structures.[4,5,8,9,13,14] Three different stages can be identified in these plots: current transient begins with a negative slope likely associated with the build up of defects within the oxide layer. This process ends with the formation of the percolation path. This progressive current reduction is usually modeled through Curie-von Schweidler law[22] or negative charge trapping.[23] The PBD stage starts with the alteration of this slope,[5] turning positive and fluctuating until the third stage occurs, stage that is characterized by a fast current runaway (Hard Breakdown or Fast Breakdown Runaway, FBD). This stage can only be measured with a high bandwidth setup and was characterized in Section II of this work (Fig. 1).

Both sets of devices show the same general features. Figure 3(a) shows the current dependence with time for the HfO_2 devices at voltages ranging from 3.5 V to 4 V while 3(b) corresponds to Al_2O_3 devices stressed at voltages ranging from 4.2 V to 5 V. Although it is not the topic of this paper, it is possible to see the influence of the initial current on the TBD and that the onset of the PBD gets shorter as the applied voltage increases, as previously reported for MOS structures.[13] Comparing Figs. 3(a) and 3(b), it is observed that the duration of PBD in Al_2O_3 is around the same value as for HfO_2 but obtained at higher applied voltages, ranging from 4.2 V up to 5 V.

Although the statistical analysis of the breakdown characteristics is not the aim of this paper, the experimental data observed in Fig. 3 show that Q_{BD} is not constant as a function of stress voltage in agreement with previous results.[13] Calculating Q_{BD} according to Ref. 12, it is observed as a small decrease of Q_{BD} as the stress voltage increase. In the case of HfO_2, Q_{BD} is 2.1×10^{-9} C, 8.5×10^{-9} C and 7.7×10^{-9} C for 4 V, 3.8 V, and 3.5 V, respectively. In the case of Al_2O_3, Q_{BD} is 1.88×10^{-11} C, 1.8×10^{-11} C, and 2×10^{-10} C for 5 V, 4.5 V, and 4.2 V, respectively.

To quantitatively evaluate the difference in the PBD evolution, the degradation rate (DR) as calculated in Ref. 3 is considered: the breakdown current growth with time is quantified through the slope in the PBD regime, dI_{BD}/dt, for each applied voltage.

Figure 3(c) shows the obtained results for DR as a function of the applied voltage. Although the dispersion is high, a general trend is observed for both sets of samples: the degradation rate increases with the applied voltage. This is in agreement with previously reported results on MOS stacks.[8,9,13] The main point of Fig. 3(c) is the difference between the two sets of devices. For similar DR values, the Al_2O_3-based MIM stacks require higher voltages (around 1 V higher) than the HfO_2-based MIM stacks.

Summarizing the results so far, a clear difference arises between the two insulators under study. Breakdown phenomenon, both in the case of PBD and FBD, requires higher voltages in Al_2O_3 for characteristic times similar to those found for the HfO_2 samples. In other words, extrapolating the trends to the same applied voltages for both sets of samples, Al_2O_3 presents smaller *DR* and longer t_r than HfO_2 samples. This result can be linked to the role played by the thermal conductivity of the insulators on the dynamics of *PBD*. In this regard, *PBD* has been recently modeled in Refs. 8 and 9 by considering the thermal processes that trigger electromigration in MOS structures under breakdown conditions. The capability of different insulating materials to transfer heat from the conductive filament to the bulk of the oxide, represented through their thermal conductivities, has a strong impact on the dynamics of *PBD* in MOS structures with different material stacks.[3,4,8–10,13] Our results show that this influence is visible for MIM structures as well. The higher thermal constant of Al_2O_3, which ranges from 20 W/mΔK to 35W/mΔK according to its composition and fabrication,[24]

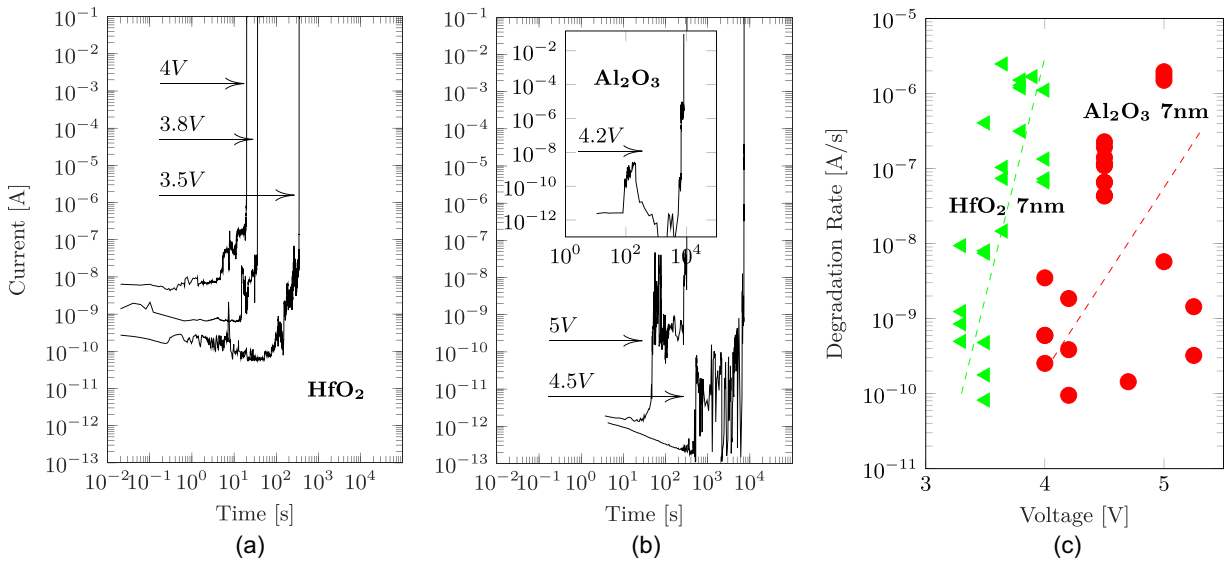

FIG. 3. Results of CVS experiments performed with a SMU. (a) and (b) are representative I-T curves for HfO_2 and A l_2O_3 samples, respectively. (c) is a scatter plot of DR values obtained from several measurements at different applied voltages.

compared to that of HfO_2 that takes values around $1W/m\Delta K$,[25] seems to be responsible for the differences in the *PBD* characteristics.

The difference between fast (at high current) and slow (at low current) PBD transients is quite noteworthy. Though the voltages are the same, the characteristic times τ (in the equation $dI_{BD}/dt = I_{BD}/\tau^3$) differ quite a bit by comparing the fast measurements taken by the current amplifier with the slow measurements acquired through the SMU. A possible explanation for such a difference may be ascribed to the different current levels. At low currents, we are in a regime of single electron tunneling through high and thin barriers. At high currents, on the other hand, we are in a regime of heavy energy loss. Therefore, since according to Ref. 8 the energy released by the carriers through the PBD spot is the cause of its growth, we may conclude that at the early stages of PDB, when the current is small, the dI_{BD}/dt is small for two reasons, i.e., since I_{BD} is small and since the energy loss is small, so that negligible electromigration takes place. At high current, on the contrary, both I_{BD} and energy loss are high, so dI_{BD}/dt is large.

In this regard, it is worth mentioning that the slow rise of current at *pA* level in Fig. 3 can be attributed to stress-induced leakage current, (SILC[26]), since at such a current level, the BD spot temperature estimated by the model of Ref. 9 is not sufficient to promote electro-migration of the fastest atomic species among those available in the contact, providing to the build-up of the BD filament. While SILC is the increased leakage that results from defects being generated everywhere within the dielectric in accordance with the percolation model,[27] PBD reflects the formation of a breakdown path created by these defects within the dielectric.[10,28] After the onset of PBD, further stress increases the current noise until Hard BD occurs. Moreover, this may explain the large dispersion in the data of Fig. 3.

A short comment on Fig. 2 is necessary. Extrapolations to high applied voltages show that rise times tend to coincide at some bias value, which can be interpreted as a case of power dissipation so high that the breakdown path reaches temperatures around the melting point of the surrounding materials (2300 K for Al_2O_3 and 3000 K for HfO_2).[8,13,24] Under this circumstance, differences between materials do not longer matter. However, for lower voltages, the difference of around 30 times between thermal conductivities provides the Al_2O_3, the capability to maintain the temperature of the BD path below the melting point for longer times.

Finally, it is relevant to consider that this result is not an artifact due to a poor structural quality of the dielectric layer. The stack quality in terms of defects (i.e., interface states, border traps, and leakage current) affects only the first phase of the I-t measurements, associated with the wear-out phase.[1,13,23] Since our data (Figs. 1–3) show that the PBD regime is driven by thermal conductivity and not by the quality of the dielectric layer, improving the quality of the latter will not affect the rise time of the *BD* transient. Considering this observation, it seems clear that the above conclusions neither rely on the quality of the high-k dielectric layer nor on the quality of their interfaces with the electrodes.

B. Characteristics of the BD path

The progressive increase of the BD current has been demonstrated to be highly localized,[5,28] where the lateral size of the leakage path increases with time as well.[29,30] Since Landauer's model[31] for mesoscopic systems has proven to be useful for modeling the electron transport in the constriction associated with the percolation path under the progressive *BD* regime,[30,32] the same model is used to analyze these MIM structures.

Although Sec. III A showed differences in the PBD of the stacks under test, it is imperative to study the characteristics of the BD path in both sets of samples in order to validate that analysis. To compare the particular features of the conductive BD filaments for both sets of devices, additional voltage-current measurements (V-I) were carried out. The use of current ramped stress allows capturing the details of the BD path growth dynamics, which is eventually driven by the interplay between lateral expansion of the filamentary path and voltage reduction, the latter being a key parameter for the degradation rate of dielectric films.[1]

Measurements on both sets of devices were carefully planned to ensure a gradual degradation of the structures. For each consecutive V–I curve, the current sweep is stopped at some prescribed values and subsequently resumed starting from a lower initial current value. The onset of breakdown is detected as a noisy behavior followed by a voltage reduction trend. In all cases, an abrupt voltage drop indicates the final evolution of the BD path. Such a sweep is very important because the physical damage caused to the device strongly depends on the maximum current that flows through the oxide layer. This has been confirmed by transfer electron microscopy (TEM) images for the SiO_2/Si system.[1] The sweeps were repeated until the structure showed signs of catastrophic dielectric breakdown.

Figures 4(a) and 4(b) show typical consecutive V-I curves for Al_2O_3- and HfO_2-based MIM stacks, respectively. It is observed that despite of different dielectric layers, the breakdown phenomenon is very similar in both structures, suggesting that the evolution of a filamentary path is, at first order, identical for both insulators. The curves in Fig. 4 were fitted using the Landauer formula, which has been extensively used to model the dielectric breakdown of ultra-thin SiO_2 layers in MOS structures,[29] and more recently it has been introduced to characterize the conduction modes of MIM stacks in the framework of the RS phenomenon.[30,32–34] This model considers a potential barrier that represents the bottom of the first energy sub-band associated with the quantization of the transverse electron momentum at the narrowest point along the filamentary path. The total current depends on the transmission coefficient through this barrier. This coefficient depends on the shape of the confinement potential. According to Landauer's approach for mesoscopic conduction under finite applied bias[31] and considering an inverted parabolic confinement potential as the one represented in Fig. 5, the current in high resistance state (HRS) reads[11,33]

$$I_{HRS} = \frac{4e}{h\alpha}\frac{\exp(-\alpha\Phi)}{\sin c(\pi kT\alpha)}\sin h\left(\frac{\alpha eV}{2}\right), \quad (1)$$

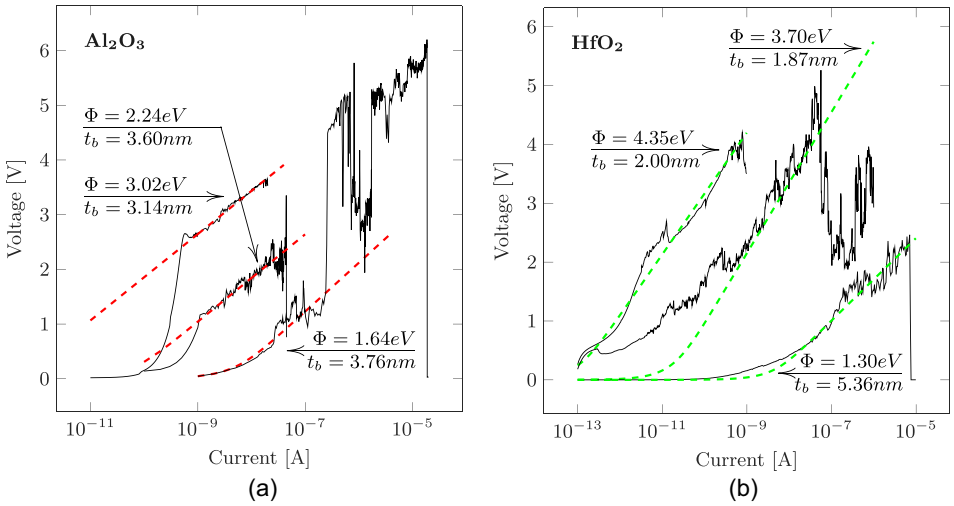

FIG. 4. Successive V-I sweeps and Landauer model fit for both material stacks. (a) corresponds to Al_2O_3 based structures and (b) to HfO_2 based.

$$\alpha = \frac{t_b \pi}{h}\sqrt{\frac{2m^*}{\Phi}}, \tag{2}$$

where Φ is the barrier height, t_b the barrier width, e the electron charge, k the Boltzmann's constant, h the Planck's constant, and T the room temperature. In Fig. 5, P is the transmission probability. The model assumes that the applied bias has no influence on the barrier shape.[22,30–33] Moreover, expression 1 is valid for applied voltages lesser than twice the value of the barrier height (in Volts),[31] as it is for this work. For more insight into this model, the reader is referred to Refs. 32–34.

Using Φ and t_b as fitting parameters, expression 1 was fitted to the experimental I-V and V-I curves. The results are shown as dashed curves superimposed to the experimental data in Figs. 4(a) and 4(b). In both cases, successive sweeps evolve from high resistance characteristics (curves on the left of the plot with lower currents) towards lower resistance states (curves on the right of the plot with higher currents) as the degradation proceeds. The results of each fit for both materials are plotted together in Fig. 6, which shows the evolution of the barrier height (ϕ) and width (t_b) with the maximum current reached during the corresponding sweep. This maximum current is a measure of the degradation level caused to the insulator.[1]

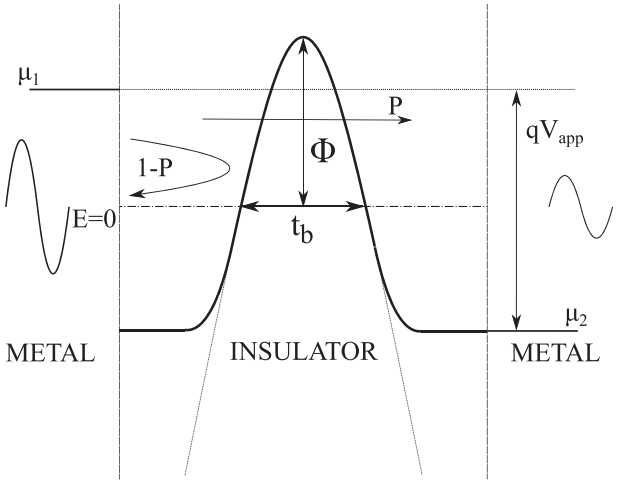

FIG. 5. Representation of the confinement potential in the narrowest point of the conductive filament. Model fitting parameters are displayed.

Fitting parameter results for Al_2O_3 appear scattered among those for HfO_2. Importantly, while the barrier width t_b does not show any particular trend with the maximum current, the barrier height Φ decreases as the current increases. Fitting values are in good agreement with the previously reported results on similar structures.[30,32,33] We can understand the evolution of the filamentary path as a reduction of the barrier height for successive current or voltage sweeps, while maintaining its width constant as suggested in Ref. 32.

It is worth noting that the same analysis was performed on I-V curves. Fitting parameters were extracted for many devices, indicating the same general behavior observed in the V-I curves (results not shown). In this case, for successive voltage sweeps, the current was monitored with a current compliance that was increased by decades (100μA, 1mA, 10mA, 100mA) in successive sweeps.

Considering the interpretation that PBD is characterized by the migration of atoms of the contacts towards the oxide by an electro-migration process,[9,10,23] the physical origin of the evolution of the barrier parameters with the maximum applied current could be linked to this effect.

Particularly, the evolution of the barrier parameters observed in Fig. 6 agrees with independent results in MOS stacks using X-ray Photoelectron Spectroscopy (XPS) regarding the amount of material from the electrodes that moves towards the oxide layer by the electromigration effect during the BD event. A power law dependence of this magnitude as a function of the compliance limit in the BD event has been reported for Al_2O_3 layers in *InGaAs* based-MOS stacks.[10]

A comment on the nature of the transport process for PBD conduction when using the Landauer's model should be made at this point. Being the BD growth rate affected by the thermal conductivity of the dielectric layer, it is reasonable to assume that the heat dissipation occurs at the BD spot center. In the literature, Takagi *et al.*[35] have shown that the electrons tunneling through defects responsible for SILC in thin oxynitrides do lose a large fraction of their energy in the oxide. That is, the electron tunneling through oxide defects

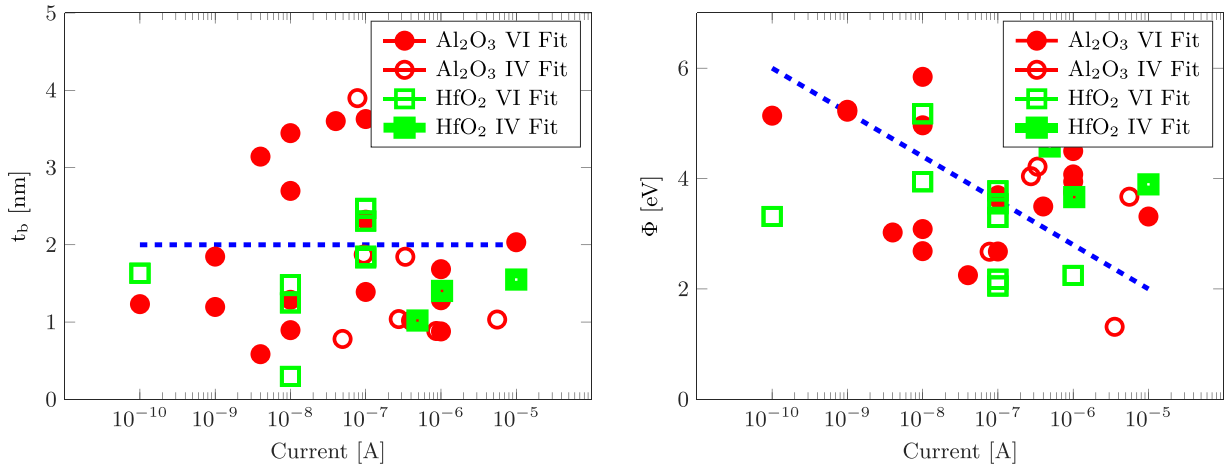

FIG. 6. Scatter plot of the obtained fitting parameter values for both sets of samples and both V-I and I-V sweeps.

is inelastic, with a large fraction of electron energy lost due to defect relaxation, as shown by Blöchl and Stathis.[36] Landauer's model used for PBD conduction can consider the Joule heating in the regions around a scattering center present in the conductive filament.[31] That is, the power due to the current flowing through the device is dissipated around this scattering center (in this case, a barrier with transmission probability P) and the energy is transferred to the surrounding lattice. Although the transport process through the constriction is inherently elastic, Soreé *et al.*[37,38] link the dissipation to the presence of phonons in the vicinity of this constriction, where inelastic processes occur.

This section has shown that both sets of samples show conductance characteristics that can be represented in terms of the same model as degradation is produced. Linking this consideration to Sec. III A of this work, it is possible to say, that although the means for carrier transport across the insulators are virtually the same for both materials, the degradation dynamics, i.e., the growth rate of the PBD, show strong differences ascribed to the thermal properties of the dielectrics, while being consistent with the physical mechanisms that describe the evolution of the conductance characteristics.

IV. SUMMARY

In this work, experiments of BD transient have been conducted on MIM stacks with different oxide materials (Al_2O_3 and HfO_2) and identical metal electrodes. Fast and slow experimental setups were used to capture the features of the different stages of PBD. Accepted metrics that quantify this event were used to compare both systems.

The use of two dielectric layers with large differences in its thermal characteristics allowed to qualitatively assess the influence of the thermal constants of the oxide layer in the dynamics of PBD.

Most contributions to this date focused on the study of MOS stacks. But since PBD is strongly associated with power dissipation, the potential role of the metal electrodes needs to be observed in MIM stacks.

It has been shown that the general behavior of PBD dynamics in MIM stacks show great resemblance to that reported for MOS stacks. This leads to the idea that the thermal mechanisms that govern PBD depend strongly on the capabilities of the insulating layers to dissipate the heat generated in the conductive filament to its surrounding atomic network, with little, or no, influence of the electrode materials.

ACKNOWLEDGMENTS

This work was funded by the Argentinean Ministry of Science and Technology (MINCyT) under Contract PICT2013/1210, the National Council for Scientific and Technical Research (CONICET) under Project PIP-11220130100077CO and the Buenos Aires Regional Faculty of the National Technological University (UTN.BA) under Project PID-UTN2014/UTI2423. The authors greatly acknowledge Dr. Eilam Yalom from the Technion Israel Institute of Technology for providing the samples.

[1]S. Lombardo, J. H. Stathis, B. P. Linder, K. L. Pey, F. Palumbo, and C. H. Tung, J. Appl. Phys. **98**, 121301 (2005).
[2]J. H. Stathis, IBM J. Res. Dev. **46**, 265 (2002).
[3]B. Linder, S. Lombardo, J. Stathis, A. Vayshenker, and D. Frank, IEEE Electron Device Lett. **23**, 661 (2002).
[4]S. Lombardo, J. H. Stathis, and B. P. Linder, Phys. Rev. Lett. **90**, 167601 (2003).
[5]R. Pagano, S. Lombardo, F. Palumbo, P. Kirsch, S. Krishnan, C. Young, R. Choi, G. Bersuker, and J. Stathis, Microelectron. Reliab. **48**, 1759 (2008).
[6]R. Waser, R. Dittmann, G. Staikov, and K. Szot, Adv. Mater. **21**, 2632 (2009).
[7]D. Ielmini, R. Bruchhaus, and R. Waser, Phase Transitions **84**, 570 (2011).
[8]F. Palumbo, S. Lombardo, and M. Eizenberg, J. Appl. Phys. **115**, 224101 (2014).
[9]F. Palumbo, M. Eizenberg, and S. Lombardo, in *2015 IEEE International Reliability Physics Symposium* (IEEE, 2015), pp. 5A.1.1–5A.1.6.
[10]F. Palumbo, P. Shekhter, K. Cohen Weinfeld, and M. Eizenberg, Appl. Phys. Lett. **107**, 122901 (2015).
[11]E. Miranda, in *45th Annual IEEE International Reliability Physics Symposium Proceedings* (IEEE, 2007), pp. 572–573.
[12]F. Palumbo, S. Lombardo, J. Stathis, V. Narayanan, F. McFeely, and J. Yurkas, in *IEEE International Reliability Physics Symposium* (IEEE, 2004), pp. 122–125.
[13]F. Palumbo, S. Lombardo, and M. Eizenberg, Microelectron. Reliab. **56**, 22 (2016).
[14]C. H. Tung, K. L. Pey, L. J. Tang, M. K. Radhakrishnan, W. H. Lin, F. Palumbo, and S. Lombardo, Appl. Phys. Lett. **83**, 2223 (2003).
[15]E. Y. Wu and J. Suñé, Microelectron. Reliab. **45**, 1809 (2005).
[16]A. Haggag, N. Liu, D. Menke, and M. Moosa, Microelectron. Reliab. **45**, 1855 (2005).

[17]E. Y. Wu and J. Suñé, IEEE Trans. Electron Devices **56**, 1433 (2009).
[18]T. Pompl and M. Röhner, Microelectron. Reliab. **45**, 1835 (2005).
[19]R.-P. Vollertsen and E. Wu, Microelectron. Reliab. **44**, 909 (2004).
[20]A. Kerber, L. Pantisano, A. Veloso, G. Groeseneken, and M. Kerber, Microelectron. Reliab. **47**, 513 (2007).
[21]W.-T. K. Chien, Y. A. Zhao, M. Zhang, and M. Li, Int. J. Reliab., Qual. Saf. Eng. **22**, 1550006 (2015).
[22]E. Miranda, C. Mahata, T. Das, and C. Maiti, Microelectron. Reliab. **51**, 1535 (2011).
[23]F. Palumbo and M. Eizenberg, J. Appl. Phys. **115**, 014106 (2014).
[24]See https://www.nist.gov/srd/srd-catalog for NIST SRD Catalog—NIST.
[25]M. Panzer, M. Shandalov, J. Rowlette, Y. Oshima, Yi. Wei Chen, P. McIntyre, and K. Goodson, IEEE Electron Device Lett. **30**, 1269 (2009).
[26]R. Degraeve, T. Kauerauf, M. Cho, M. Zahid, L. Ragnarsson, D. Brunco, B. Kaczer, P. Roussel, S. De Gendt, and G. Groeseneken, IEEE Int. Electron Devices Meet. **2005**, 408–411 (2006).
[27]R. Degraeve, B. Kaczer, and G. Groeseneken, Microelectron. Reliab. **39**, 1445 (1999).
[28]F. Palumbo, G. Condorelli, S. Lombardo, K. Pey, C. Tung, and L. Tang, Microelectron. Reliab. **45**, 845 (2005).
[29]E. Miranda, Appl. Phys. Lett. **91**, 053502 (2007).
[30]F. Palumbo, E. Miranda, G. Ghibaudo, and V. Jousseaume, IEEE Electron Device Lett. **33**, 1057 (2012).
[31]Supriyo Datta, *Electronic Transport in Mesoscopic Systems*, 1st ed., Cambridge Studies in Semiconductor Physics and Microelectronic Engineering (Cambridge University Press, 1997), p. 377.
[32]E. Miranda, C. Walczyk, C. Wenger, and T. Schroeder, IEEE Electron Device Lett. **31**, 609 (2010).
[33]F. Palumbo, E. Miranda, G. Ghibaudo, and V. Jousseaume, ECS Trans. **39**, 187 (2011).
[34]X. Lian, S. Long, C. Cagli, J. Buckley, E. Miranda, M. Liu, and J. Sune, in *13th International Conference on Ultimate Integration on Silicon (ULIS)* (IEEE, 2012), pp. 101–104.
[35]S. Takagi, N. Yasuda, and A. Toriumi, IEEE Trans. Electron Devices **46**, 335 (1999).
[36]P. E. Blöchl and J. H. Stathis, Phys. Rev. Lett. **83**, 372 (1999).
[37]B. Sorée, W. Magnus, and W. Schoenmaker, Phys. Lett. A **310**, 322 (2003).
[38]B. Sorée, W. Magnus, and W. Schoenmaker, Semicond. Sci. Technol. **19**, S235 (2004).